

Quantification of Optical Disorder due to Nanoscale Density Fluctuations in Biological Tissue: Inverse Participation Ratio (IPR) Analysis of Transmission Electron Microscopy Images for Early-Stage Cancer Detection

Prabhakar Pradhan^{1*}, Dhwani Damania¹, Vladimir Turzhitsky¹, Hemant K. Roy²,

Allen Taflove³, Vadim Backman¹

¹*Biomedical Engineering Department, Northwestern University, Evanston, IL 60208*

²*Evanston Northwestern Hospital, Evanston, IL 60201*

³*Electrical Engineering and Computer Science Department, Northwestern University,*

Evanston, IL 60208

Corresponding author: pradhan@northwestern.edu

The disorder of nanoscale mass density fluctuations of biological tissues is studied by quantifying their nanoscale light localization properties. TEM images of human tissues are used to construct corresponding effective optical lattices. Light localization properties are studied by the statistical analysis of the inverse participation ratio (IPR) of the eigenfunctions of these lattices. Our experimental results show a statistically significant increase of the average IPR value indicating an elevation of short-range nanoscale refractive index fluctuations in early carcinogenesis. Importantly, our data indicate that the increase in the nanoscale disorder represents the earliest structural alteration in cells undergoing carcinogenesis known to date.

PACS : 72.15.Rn, 73.63.-b, 68.37. E, 87.64.M-, 87.19.xj

I. Introduction: Understanding of nanoscale light localization properties in biological tissues is important for characterizing the physical properties of these systems as well as their changes in disease such as cancer [1]. Conventional light microscopy has been widely used to study optical properties of biological systems, but their sensitivity to detect the changes at the nanoscale is limited by diffraction limited resolution [2,3]. Nanoscale resolution transmission electron microscopy (TEM) imaging technique has been widely used to visualize the nano- and micro-structures in biological samples [4]. The quantitative information encoded in TEM grayscale images, in particular their subtle short-range nanoscale fluctuations and correlations and their changes in disease, however, are poorly understood.

In this paper we report, for the first time, the quantification of the nanoscale mass density fluctuations in human tissues by studying their light localization properties via TEM image analysis. The high resolution of the TEM imaging allows imaging nanoscale fluctuations of the mass densities of thin slices (~50-100 nm) of tissue samples [4]. The TEM images from tissues are projected to their corresponding effective optical lattices via the construction of the effective tissue mass densities, and the optical eigenfunctions of these lattices are obtained (detailed in Sec.III). IPR of an eigenfunction E (normalized) is defined as $IPR = \int |E(r)|^4 d\vec{r}$. The statistical properties of IPR are important measures of the localization of light in an optical lattice (ordered or disordered). The average value of IPR for a uniform lattice is a fixed universal number and the value increases from the uniform to disordered lattice with the increase in the degree of the disorder. This has been well studied in condensed matter physics for characterization of localization and quantum hall effects [5,6,7].

As an illustration of the potential of IPR analysis we study the changes in light-localization properties of human rectal tissues in early colon carcinogenesis providing previously unattainable

information about early precancerous nanoscale changes in tissues. It is now well understood that morphological changes at the micron and supramicron scales (i.e. detectable via conventional microscopy) in tissue are prominent in later stages of carcinogenesis (i.e. dysplasia) and result from multiple genetic and epigenetic alterations. Cellular changes in the initial stages of carcinogenesis, however, are neither well studied nor are easily detectable. Here, we report the change in the nanoscale disorder properties of cytologically normal human rectal mucosal tissues in the presence of precancerous adenomatous polyps in the colon. Our experimental results show that the IPR properties of such tissues, said to be in the field of the precancerous colonic adenomas, are significantly statistically different than the IPR properties of the rectal mucosa tissues from healthy individuals [8].

II. Sample Preparation and TEM Imaging: Tissue samples of rectal biopsies from macroscopically and microscopically normal-appearing mucosa were acquired from 10 human subjects at the time of their colonoscopy in accordance with standard clinical practice. Five patients harbored precancerous adenomatous polyps elsewhere in their colon while another five patients were adenoma free. Tissue samples went through the following steps: fixation, staining, embedding, sectioning, and finally TEM imaging, as per standard protocols. Biopsy samples were first placed in Karnovsky's fixative for 2 weeks to preserve structure. The fixative consists of 0.1M phosphate buffered solution containing 5% glutaraldehyde and having a pH between 7.2 and 7.4. As per a standard protocol, the samples were stained with osmium tetroxide (OsO_4), dehydrated and then embedded in resin containing 36% ERL 4221, 12% diglycidyl ether of polypropyleneglycol (DER 736), 51% nonenyl succinic anhydride (NSA), and ~1% dimethylaminoethanol (DMAE) by mass. Samples were then sectioned with an ultra-microtome to

a thickness of 70nm and imaged with an 80KeV TEM [4]. 50 TEM images of tissues (early precancerous) were obtained from 5 patients (10 images/patients) who were found to have adenomatous polyps (precancerous changes), and other 50 TEM images from tissues (normal) were obtained from 5 patients (10 images/patients) with no colonic dysplasia. Representative TEM micrographs obtained are shown in Fig. 1(a, b).

III. Projection of a TEM image to an optical lattice and inverse participation ratio (IPR) calculation: The TEM grayscale intensity I_{TEM} decays exponentially with the thickness of the sample for a uniform sample, where the decay constant is a function of the mass density [4]. The exponential decay can be approximated as a linear decay for a very thin sample. TEM studies of thin layers of nanoscale dielectric beads have shown that grayscale I_{TEM} intensity is linearly proportional to the mass density of the beads [9,10]. For a very thin tissue sample, we can assume that the grayscale TEM image intensity at any lattice point (x,y) (Figs.1(a, b)) $I_{TEM}(x, y)$ is linearly proportional to the biomass $M(x, y)$ present in the corresponding tissue voxel around the lattice point (dimension: 10nm×10nm in xy plane, 70nm along z direction) of the tissue slice. Presently there is no well known universal functional relationship between the mass and the refractive index for all types of materials. We consider that there exists a functional (analytic) relationship between the refractive index and the tissue biomass for the biological sample we studied. However, we want to stress here that the exact functional form is not important for our present analyses. Note that the constructed optical lattice is an effective lattice of the tissue in the presence of contrast agent from the sample preparation process of the TEM imaging. Therefore, we further consider that the absorption of the contrast agent by the thin tissue voxel is also linearly

proportional to the biomass present in the voxel. Considering that the refractive index $n(x, y)$ of a voxel is functionally proportional to its bio mass, we can write:

$$n(x, y) = f(M(x, y)) = f(I_{TEM}(x, y)) \quad (1)$$

We assume the form of the TEM gray scale pixel image intensity as follows,

$$I_{TEM}(x, y) = I_0 + \Delta I_{TEM}(x, y), \quad (2)$$

where I_0 is the mean background of the whole TEM sample and $\Delta I_{TEM}(x, y)$ is the fluctuating part of the intensity around a point (x, y) of the pixel. Then, the refractive index of a tissue voxel from the corresponding TEM pixel can be written as:

$$n(x, y) = n_0 + \Delta n(x, y) = f(I_{TEM}(x)) = f_0 + f'_0 \times \Delta I_{TEM}(x, y), \quad (3)$$

where n_0 is the constant background part of the full sample and $\Delta n(x, y)$ is the fluctuating part of the refractive index in the pixel of the constructed optical lattice. It can be shown that the effective optical potential of an optical lattice ε_i has the following form [11],

$$\varepsilon_i \propto \Delta n(x, y) / n_0 = (\Delta I_{TEM}(x, y) / I_0) \times (I_0 \times f'_0 / f_0), \quad (4)$$

where $\Delta I_{TEM}(x, y) \ll I_0$ and $\Delta n(x, y) \ll n_0$ (e.g., for tissue, $n_0=1.33-1.38$ and $\Delta n=.01-.1$) [12].

We then calculated the exact eigenfunctions ($E_i(x, y)$, $i=1-N$) of each 2D pixel of optical sample size $L \times L$ by solving the electromagnetic wave equation for the electric field in the lattice using a disorder tight-binding model [13,14].

Tight-Binding model construction: To quantify the disorder properties of the TEM images, we have carried out numerical calculations of the Anderson disorder tight-binding model (TBM). TBM has been well studied and proven to be a good model for describing single-electron states or optical localized states of systems of any geometry and disorder. We consider one optical state of a photon per lattice site, and the inter lattice site hoppings are restricted to the nearest neighbors only. Such a Hamiltonian can be written as [13,14]:

$$H = \sum_i \varepsilon_i |i\rangle\langle i| + t \sum_{\langle ij \rangle} |i\rangle\langle j| + |j\rangle\langle i|, \quad (5)$$

where $\varepsilon_i \propto \Delta n(x, y) / n_0$ is the i -th lattice site energy, $|i\rangle$ and $|j\rangle$ are the optical wavefunctions at the i -th and j -th lattice sites, respectively, $\langle ij \rangle$ indicates the nearest neighbors, and t is the overlap integral between the sites i and j .

In our analyses, for short-length refractive index fluctuations, a large TEM micrograph of $15.8\mu\text{m} \times 15.8\mu\text{m}$ (as shown in Fig. 1 (a, b)) is virtually cut into $77\text{nm} \times 77\text{nm}$ to $308\text{nm} \times 308\text{nm}$ samples or IPR-pixels. To project the TEM image to the tight binding model, first the fluctuating part of every grayscale point of the TEM image is considered as proportional to the onsite optical energy ε_i (i.e., Eq.(3)). The optical potential ε_i is then rescaled such that its mean is same as the hopping parameter, i.e. $t = \text{mean}(\varepsilon_i)$, and we further consider $(I_0(x, y) f'_0 / f_0) / t = \text{constant} = 1$, without any loss of generality. We define sample length as L (in nm), lattice size as L_a units (dimension

less), and unit lattice length as a (in nm), such that $L = L_a \times a$. The eigenfunctions of each pixel of size $L \times L$ are then calculated. The average value of the IPR of an IPR-pixel, can be written as:

$$\langle IPR(L) \rangle_{Pixel} = \frac{1}{N} \sum_{i=1}^N \int_0^L \int_0^L E_i^4(x, y) dx dy, \quad (6)$$

where E_i is the i^{th} eigenfunction of the Hamiltonian in Eq.(5) of an optical lattice (i.e. an IPR-pixel) size $L \times L$, $N = L_a^2$ ($L_a = L/a$, $a = dx = dy$) is the total number of the eigenfunctions, and $\langle \dots \rangle_{Pixel}$ denotes averaged over all the N eigenfunctions of the IPR-pixel. By the construction of each IPR-pixel, we are mainly considering the fluctuating part of the n relative to its average background as the rescaled potential.

IV. Results: IPR analysis of the TEM images: Figures 1(a, b) show the typical TEM grayscale images of normal tissue and early precancerous tissue. The corresponding IPR images (IPR-pixel by pixel, IPR-pixel dimension is 262nm×262nm, i.e., lattice size is 20×20) are shown Fig.1 (a' and b'). The IPR images clearly indicate two different disorder states for tissues from normal and early precancerous patients.

To illustrate the potential of the IPR technique in detecting early carcinogenesis, we have carried out a pilot human study. We calculated the average properties of the IPR of microscopically normal-appearing tissues obtained in the rectum from normal and early precancerous patients (as described in Sec.II). Total 100 TEM images were analyzed (50 TEM

images from each group). Each TEM micrograph dimension is $15.8\mu\text{m}\times 15.8\mu\text{m}$ and the corresponding lattice size is 2048×2048 .

Figure 2 shows the $\langle IPR(L) \rangle_{\text{Pixel}}$ distributions of normal and precancerous tissues for different IPR-pixel sizes: $L\times L=77\times 77\text{nm}^2$, $154\times 154\text{nm}^2$, $231\times 231\text{nm}^2$, and $308\times 308\text{nm}^2$ (i.e., lattice sizes ($L_a=L/a$, $a=7\text{nm}$) $L_a\times L_a= 10\times 10$, 20×20 , 30×30 , and 40×40 , respectively). This illustrates a distinct separation between the two groups of patients. The average and the standard deviation of the distribution, both increase with the sample (i.e., lattice) size.

Figure 3 shows $\langle\langle IPR(L) \rangle_{\text{Pixel}} \rangle$ versus L plots for three different cases: (i) uniform lattice, (ii) normal tissues, and (iii) early precancerous tissues. The ensemble averaging is denoted by $\langle \rangle$ were performed over 500,000 IPR-pixels for the IPR-pixel length $L=77\text{nm}$ (i.e., $L_a=10$) and over 31250 IPR-pixels for pixel length $L=308\text{nm}$ (i.e., $L_a=40$) for each group of patients. The $\langle\langle IPR(L) \rangle_{\text{Pixel}} \rangle$ for the uniform sample (i.e. background) increases with increased L and then it saturates to a value (universal) at IPR ~ 2.5 around the lattice size $L_a=40$ (i.e., $L=308\text{nm}$, $N=40\times 40$). The three curves in Fig. 3 clearly show that the $\langle\langle IPR(L) \rangle_{\text{Pixel}} \rangle$ value is highest for the early precancerous tissues. For example, $\langle\langle IPR(L) \rangle_{\text{Pixel}} \rangle$ values (in Fig. 3) for uniform background, normal tissues, and early precancerous tissues are ~ 2.5 , 3.053 , and 3.196 , respectively. The higher value of the average IPR corresponds to the higher disorder strength due to the larger nanoscale fluctuations in the optical lattices. The IPR of a disordered sample is a function of the light localization length, i.e. a function of the optical disorder strength. Fig. 3 (Inset) shows the standard deviation $\sigma(\langle IPR(L) \rangle_{\text{Pixel}})$ versus L plots for the early precancerous tissues is higher and it increases faster than that of the normal tissues. Importantly, Fig.3 also shows the ratio $\sigma(\langle IPR(L) \rangle_{\text{Pixel}}) / \langle\langle IPR(L) \rangle_{\text{Pixel}} \rangle$ value increases much faster with increasing L for

the early precancerous tissues relative to the normal tissues (e.g. the value of the ratio for early precancerous tissues is ~ 2 times larger than the ratio for the normal tissues at $L=308\text{nm}$). This indicates higher disorder strength for early precancerous tissues relative to the normal tissues. The fast increase of the above ratio is attributed to the long tails in the IPR distributions.

V. Discussion and Conclusion: We report an IPR analysis to quantify, for the first time, the short-range nanoscale light localization properties of mass density fluctuation in human tissues via their TEM image analysis. Importantly, we show the increase in disorder of the nanoscale refractive index fluctuations in short length scales (i.e. increase in the average IPR value) for histologically normal mucosa in the earliest stage of carcinogenesis. Due to the very large number of samples (e.g., for $L=308\text{nm}$, the number of samples or IPR-pixels = 31,250), the result is highly statistically significant (Student t -test, two-tailed p -value = 5.95×10^{-38}). This is the first imaging and analysis technique that enable imaging and quantification of the “field effect” of colon carcinogenesis [8]. Until now, no morphological alterations in this earliest stage of carcinogenesis have been reported and only molecular (e.g., genetic, epigenetic, and proteomics) alterations have been described. The increase in the nanoscale disorder reported here represents the earliest morphological alteration in carcinogenesis known to date.

We have assumed a mean absorption coefficient of the tissue biomass to absorb TEM contrast agent and linearity between TEM greyscale image fluctuations and the effective refractive index fluctuations, in our analysis. These two assumptions are plausible for a thin sample and for weak mass density fluctuations. We hope that IPR study of TEM images will have potential applications for tissue/cell characterizations in basic biological research as well as medical applications in early-stage cancer detection.

Samples were acquired in accordance to the institutional review board (IRB) at Evanston Northwestern Healthcare. This work is supported in part by NIH grants R01 EB003682, R01 CA112315, NSF grant CBET-0733868. We also thank the Northwestern University TEM facilities FOB for the TEM images.

References

- [1] D. S. Coffey, Nat. Med. **4**, 882-885 (1998).
- [2] M. Born, and E. Wolf, *Principles of optics : electromagnetic theory of propagation, interference and diffraction of light* (Cambridge University Press, Cambridge ; New York, 1999).
- [3] D. J. Stephens and V.J. Allan, Science **300**, 82 (2003).
- [4] J. J. Bozzola, L. Dee, *Electron Microscopy : Principles and Techniques for Biologists* (Jones and Bartlett, 1999).
- [5] P. Pradhan and S. Sridhar, Phys. Rev. Lett. **85**, 2360 (2000); P. Pradhan and S. Sridhar, Pramana J. Phys. **58**, 333(2002).
- [6] T. Schwartz, *et al.*, Nature **446**, 52 (2007).
- [7] V. N. Prigodin and B. L. Altshular, Phys. Rev. Lett, **80** 1944 (1998) .
- [8] L. Chen, *et al.*, Cancer Res. **64**, 3694 (2004).
- [9] E. Zeitler and G. F. Bahr, J. Appl. Phys. 33, 847 (1962).
- [10] M. Loferer-Kröbßbacher, J. Klima, and R. Psenner, Appl. and Enviorn. Microbiol. **64**, 688(1998).
- [11] P. Pradhan, Phys. Rev. B. **74**, 085107 (2006).
- [12] J. M. Schmitt and G. Kumar, Opt. Lett. **21**, 1310 (1996).
- [13] P. A. Lee and D. S. Fisher, Phys. Rev. Lett. **47**, 882 (1981).
- [14] B. Kramer and A. MacKinnon, Rep. Prog. Phys. **56**, 1469 (1993).

Figures and captions:

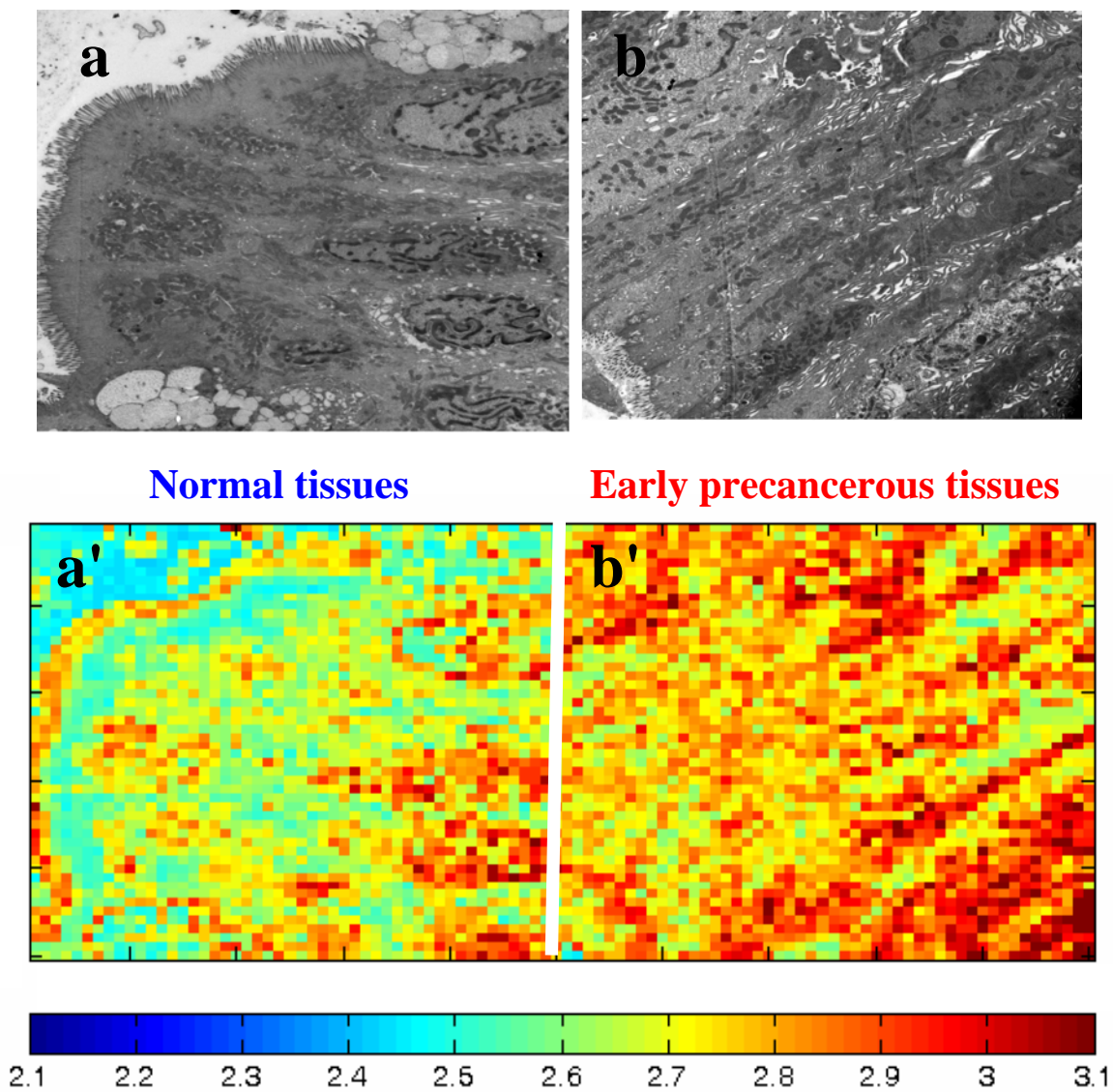


Figure 1: Representative TEM images of (a) normal rectal tissue and (b) rectal tissue in the field of precancerous colonic adenomatous polyps, and the corresponding IPR-pixel images are (a') and (b'). Each TEM image size (full) is $15.8\mu\text{m} \times 15.8\mu\text{m}$, and each IPR-pixel size is $262\text{nm} \times 262\text{nm}$ with its average IPR value $\langle IPR(L) \rangle_{\text{pixel}}$ at $L=262\text{nm}$.

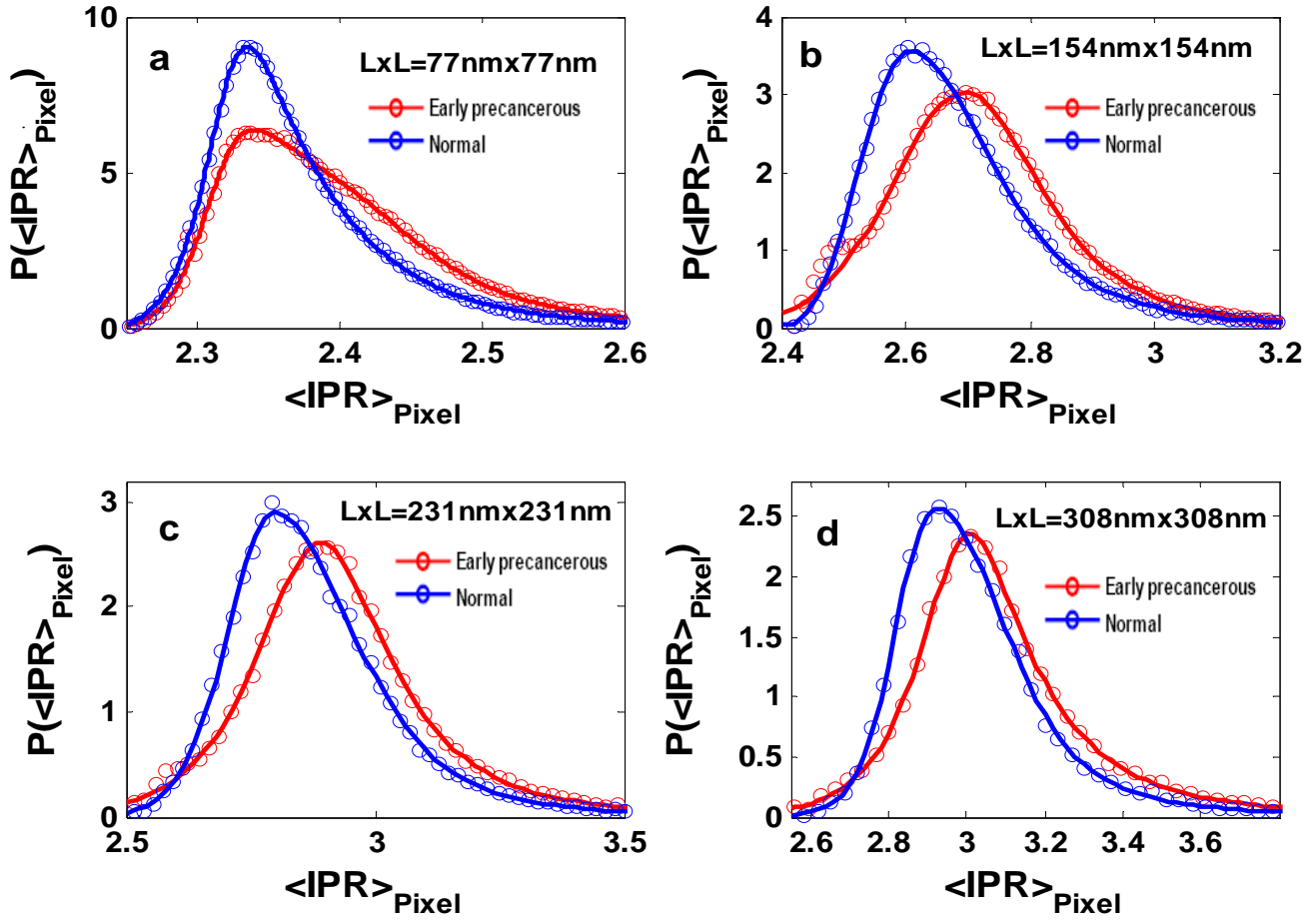


Figure 2: Relative $\langle IPR(L) \rangle_{Pixel}$ distributions (ensemble) at different sample (i.e. IPR-pixel) sizes $L \times L =$: (a) $77 \times 77 \text{ nm}^2$, (b) $154 \times 154 \text{ nm}^2$, (c) $231 \times 231 \text{ nm}^2$, and (d) $308 \times 308 \text{ nm}^2$ for normal rectal tissues and early precancerous rectal tissues.

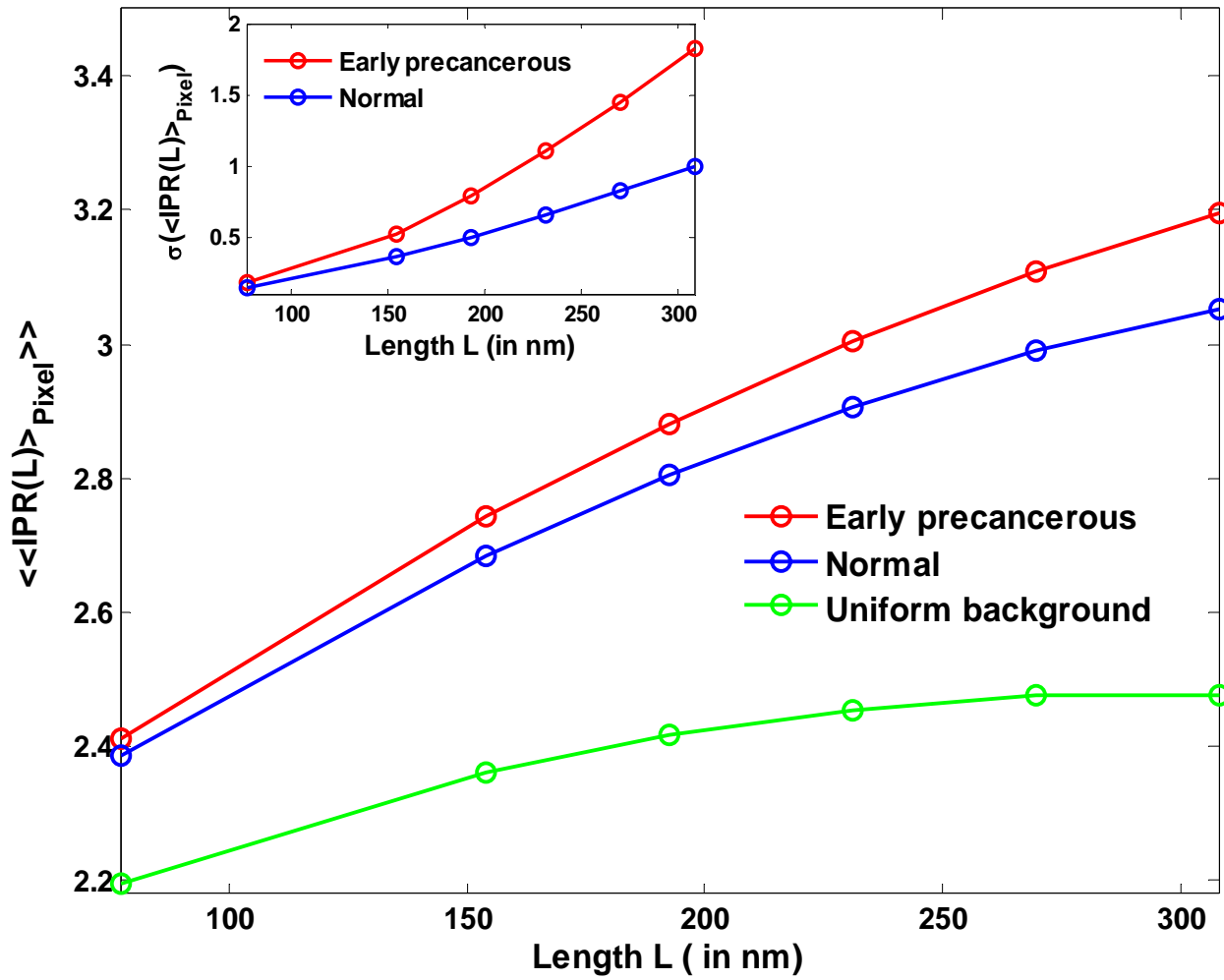


Figure 3: The ensemble average values of the IPR-pixel (or sample) $\langle\langle IPR(L) \rangle_{Pixel}\rangle$ versus L (in nm) plots for : (i) uniform sample (or background), (ii) normal tissues, and (iii) early precancerous tissues. Inset, standard deviation $\sigma(\langle IPR(L) \rangle_{Pixel})$ versus L (in nm) plots for normal tissues and early precancerous tissues.